International Journal of Applied Engineering Research ISSN 0973-4562 Volume 13, Number 6 (2018) pp. 3772-3783

Feedback Control and Stability of the Van der Pol Equation Subjected to External and Parametric Excitation Forces

M. Sayed[1, 2], S. K. Elagan[1], M. Higazy[1, 2] and M. S. Abd Elgafoor[3]

[1]*Department of Mathematics and Statistics, Faculty of Science, Taif University, Taif, El-Haweiah, P.O. Box 888, Zip Code 21974, Kingdom of Saudi Arabia*

[2]*Department of Engineering Mathematics, Faculty of Electronic Engineering, Menoufia University, Menouf 32952, Egypt.*

[3]*Department of Mathematics, College of Applied Medical Sciences, Turabah, Taif University, Kingdom of Saudi Arabia.*

Abstract

The main aim of this paper is to find analytical and numerical study to investigate the vibration and stability of the Van der Pol equation subjected to external and parametric excitation forces via feedback control. An approximate solution is obtained applying the multiple scales perturbation technique to analyze the nonlinear behavior of this model. The stability of the system is investigated applying Lyapunov first method. The effects of the different parameters on the system behavior are studied. For positive and negative values of the nonlinear parameters, the curves are bent to right or left leading to the occurrence of the jump phenomena and multi-valued amplitudes produce either hard or soft spring respectively. The numerical simulations are performed to demonstrate and validate the accuracy of the approximate solutions. Analyses showed that all predictions from analytical solutions are in excellent agreement with the numerical integrations.

Keywords: vibration suppression, feedback control, stability, jump phenomena

AMS Subject Classification: 70K05, 70K20, 93C10, 93D20

INTRODUCTION

Vibration, occurring in most machines, vehicles, structures, building and dynamic systems is undesirable phenomenon, not only because of the resulting unpleasant motions, the dynamic stresses which may lead to fatigue and failure of the structure or machine, the energy losses and reduction in performance which accompany vibrations, but also because of the produced noise. Active and passive control is used to eliminate or reduce the vibration to minimum level.

Active control is now commercially available for reducing vibrations offering better comfort with less weight than traditional passive technologies. The Van der Pol equation is of great interest because it can serves as a basic model for self-excited oscillations in many disciplines [1–3]. The studies on chaotic motion in systems of ϕ^4 Van der Pol oscillators have revealed various types of interesting behaviors [4–7]. Liu and Yamaura [8] studied the dynamics of a ϕ^6 Van der Pol oscillator subjected to an external excitation. Numerical analysis are presented to observe its periodic and chaotic motions, and a method called Multiple-prediction Delayed Feedback Control is proposed to control chaos effectively via periodic feedback gain. Ruihong et al. [9] investigated the dynamical behavior of the ϕ^6 Van der Pol system subjected to both external and parametric excitation. The effect of parametric excitation amplitude on the routes to chaos is studied by numerical analysis. Warminski et al. [10] discussed active suppression of nonlinear composite beam vibrations by selected control algorithms. Wang et al. [11] presented theoretical and experimental study of active vibration control of a flexible cantilever beam using piezoelectric actuators. Shan et al. [12] studied slewing and vibration control of a single link flexible manipulator by positive position feedback controller. El-Ganaini et al. [13] applied positive position feedback active controller to reduce the vibration of a nonlinear system. They found that the analytical and numerical solutions are in good agreement. Amer et al. [14] Studied the dynamical system of a twin-tail aircraft which described by two coupled nonlinear differential equations having both quadratic and cubic nonlinearities. They used two simple active control laws based on the linear negative velocity and acceleration feedback. Eissa and Sayed [15-17] and Sayed [18], studied the effects of different active controllers on simple and spring pendulum at the primary resonance via negative velocity feedback or its square or cubic. Sayed and Kamel [19, 20] investigated the effect of different controllers on the vibrating system and the saturation control of a linear absorber to reduce vibrations due to rotor blade flapping motion. The stability of the obtained numerical solution is investigated using both phase plane methods and frequency response equations. Eissa et al. [21] applied a proportional-derivative controller to the nonlinear magnetic levitation system subjected to external and parametric excitations. They studied the effects of proportional and derivative gains to give the best performance for the system.

MATHEMATICAL ANALYSIS

The general form of the Van der Pol Oscillator model with external and parametric excitation forces is given by a second-order non-autonomous differential equation as follows:

$$\begin{aligned}\ddot{X} - \mu(1-X^2)\dot{X} + \omega^2 X + \lambda X^3 + \beta X^5 \\ = f_1 \cos\Omega_1 t + X f_2 \cos\Omega_2 t + T\end{aligned} \quad (1)$$

where X is the position coordinate, which is a function of the time t, and μ is a scalar parameter indicating the nonlinearity

and the strength of the damping, $T = -\varepsilon G\ddot{X}$ active control (negative acceleration feedback) and λ, β are the nonlinear parameters, f_1 and f_2 are the external and parametric of the excitation forces, ω is the natural frequency, Ω_1, Ω_2 are the forcing frequency of the system. The damping coefficient, non-linear parameters and excitation forces are assumed to be

$$(\mu, \lambda, \beta, f_1, f_2) = (\varepsilon\hat{\mu}, \varepsilon\hat{\lambda}, \varepsilon\hat{\beta}, \varepsilon\hat{f_1}, \varepsilon\hat{f_2}) \qquad (2)$$

where ε is a small perturbation parameter and $0 < \varepsilon << 1$. The parameters $\hat{\mu}, \hat{\lambda}, \hat{\beta}, \hat{f_1}, \hat{f_2}$ are of the order 1. The method of multiple time scales [22-24] is used to obtain a uniformly valid, asymptotic expansion of the solution for equation (1) in the case of simultaneous primary and principal parametric resonance case where $\Omega_1 \approx \omega$, $\Omega_2 \approx 2\omega$. We seek a first order uniform expansion for the solutions of equations (1) in the form

$$X(t, \varepsilon) = x_0(T_0, T_1) + \varepsilon x_1(T_0, T_1), \qquad (3)$$

where $T_0 = t$ is referred to as the fast time scale characterizing motions with natural and excitation frequencies, and $T_1 = \varepsilon t$ as the slow time scale characterizing modulation and phases of the two modes of vibration. The first and second time derivatives can be written as:

$$\frac{d}{dt} = \frac{\partial}{\partial T_0}\frac{\partial T_0}{\partial t} + \frac{\partial}{\partial T_1}\frac{\partial T_1}{\partial t} = D_0 + \varepsilon D_1,$$
$$\frac{d^2}{dt^2} = D_0^2 + 2\varepsilon D_0 D_1 + \varepsilon^2 D_1^2 \qquad (4)$$

where $D_n = \partial/\partial T_n$, $n = 0, 1$. In this paper, only T_0 and T_1 are considered so that the second-order and higher-order terms, with respect to ε, are neglected. Substituting equations (2)-(4) into equation (1), and equating the coefficients of similar powers of ε, one obtain the following set of ordinary differential equations:

Order ε^0:

$$(D_0^2 + \omega^2)x_0 = 0 \qquad (5)$$

Order ε^1:

$$(D_0^2 + \omega^2)x_1 = -2D_0D_1x_0 + \hat{\mu}(1 - x_0^2)D_0x_0 - \hat{\lambda}x_0^3 - \hat{\beta}x_0^5 + \hat{f}_1\cos(\Omega_1T_0) + x_0\hat{f}_2\cos(\Omega_2T_0) - G D_0^2x_0 \qquad (6)$$

The general solution of equation (5), can be written in the form

$$x_0 = A(T_1)\exp(i\,\omega T_0) + \bar{A}(T_1)\exp(-i\,\omega T_0) \qquad (7)$$

where A is undetermined complex function, which can be determined by imposing the solvability condition at the next approximation by eliminating the secular and small-divisor terms, the over bar denotes complex conjugate. Substituting equation (7) into equation (6), we obtained

$$(D_0^2 + \omega^2)x_1 = i\omega(-2D_1A + \hat{\mu}A)\exp(i\omega T_0) - \hat{\lambda}[A^3\exp(3i\omega T_0) + 3A^2\bar{A}\exp(i\omega T_0)]$$
$$-i\omega\hat{\mu}\left[A^3\exp(3i\,\omega T_0) + 2A^2\bar{A}\exp(i\,\omega T_0) + \bar{A}^2A\exp(-i\,\omega T_0)\right]$$
$$-\hat{\beta}\left[A^5\exp(5i\,\omega T_0) + 5A^4\bar{A}\exp(3i\,\omega T_0) + 10A^3\bar{A}^2\exp(i\,\omega T_0)\right]$$
$$+\frac{\hat{f}_1}{2}\exp(i\,\Omega_1T_0) + \frac{\hat{f}_2}{2}\left[A\exp(i\,(\Omega_1 + \omega)T_0) + \bar{A}\exp(i\,(\Omega_1 - \omega)T_0)\right]$$
$$+\omega^2AG\exp(i\,\omega T_0) + cc \qquad (8)$$

where *cc* stands for the complex conjugate of the preceding terms. To describe quantitatively the closeness of the resonances, we introduce the detuning parameters σ_1 and σ_2 according to

$$\Omega_1 = \omega + \varepsilon\sigma_1\ ,\ \Omega_2 = 2\omega + \varepsilon\sigma_2 \qquad (9)$$

Substituting Eq. (9) into Eq. (8) and eliminating the secular and small divisor terms from x_1, we get the following

$$2i\omega D_1A - i\hat{\mu}\omega A + i\hat{\mu}\omega A^2\bar{A} + 3\hat{\lambda}A^2\bar{A} + 10\hat{\beta}\,A^3\bar{A}^2 - \omega^2AG - \frac{\hat{f}_1}{2}\exp(i\sigma_1T_1) - \frac{\hat{f}_2}{2}\bar{A}\exp(i\,\sigma_2T_1) = 0 \qquad (10)$$

To analyze the solution of Eq. (10), it is convenient to express the $A(T_1)$ in the polar form as

$$A(T_1) = \frac{1}{2}a(T_1)e^{i\,\gamma(T_1)} \qquad (11)$$

where *a* and γ are unknown real-valued functions. Inserting Eq. (11) into Eq. (10) and separating real and imaginary parts, we have

$$a' = \frac{\mu}{2}a - \frac{\mu}{8}a^3 + \frac{f_1}{2\omega}\sin\varphi_1 + \frac{f_2}{4\omega}a\sin\varphi_2 \qquad (12)$$

$$a\gamma' = -\frac{\omega G}{2}a + \frac{3\lambda}{8\omega}a^3 + \frac{10\beta}{32\omega}a^5 - \frac{f_1}{2\omega}\cos\varphi_1 - \frac{f_2}{4\omega}a\cos\varphi_2 \qquad (13)$$

where, $\varphi_1 = \sigma_1T_1 - \gamma$ and $\varphi_2 = \sigma_2T_1 - 2\gamma$ (14)

Then, it follows from Eq. (14) that

$$\gamma' = \sigma_1 - \varphi_1' = \frac{1}{2}(\sigma_2 - \varphi_2') \quad (15)$$

The first approximation periodic solution in this case can be written as

$$X = a\cos(\Omega t - \varphi_1) + O(\varepsilon), \quad (16)$$

STABILITY ANALYSIS

Form the system of Eqs. (12)-(13) to have stationary solutions; the following conditions must be satisfied:

$$a' = \varphi_1' = \varphi_2' = 0 \quad (17)$$

It follows from Eq. (15) that

$$\gamma' = \sigma_1 = \frac{\sigma_2}{2} = \sigma \quad (18)$$

Hence, the system steady state solutions of Eqs. (12)-(13) are given by

$$\frac{\mu}{2}a - \frac{\mu}{8}a^3 + \frac{f_1}{2\omega}\sin\varphi_1 + \frac{f_2}{4\omega}a\sin\varphi_2 = 0 \quad (19)$$

$$a\sigma + \frac{\omega G}{2}a - \frac{3\lambda}{8\omega}a^3 - \frac{10\beta}{32\omega}a^5 + \frac{f_1}{2\omega}\cos\varphi_1 + \frac{f_2}{4\omega}a\cos\varphi_2 = 0 \quad (20)$$

Solving the resulting algebraic equations, the frequency response equation can be obtained in the form

$$\left(\frac{\mu}{2}a - \frac{\mu}{8}a^3\right)^2 + \left(a\sigma + \frac{\omega G}{2}a - \frac{3\lambda}{8\omega}a^3 - \frac{10\beta}{32\omega}a^5\right)^2 - \frac{f_1^2}{4\omega^2} - \frac{f_2^2}{16\omega^2}a^2 - \frac{f_1 f_2}{4\omega^2}a\cos(\varphi_1 - \varphi_2) = 0 \quad (21)$$

Non-linear Solution

To determine the stability of the fixed points, one lets

$$a = a_0 + a_1 \text{ and } \varphi_m = \varphi_{mo} + \varphi_{m1} \quad (m = 1, 2) \quad (22)$$

where a_0 and φ_{mo} are the solutions of Eqs. (19)-(20) and a_1, φ_{m1} are perturbations which are assumed to be small compared to a_0 and φ_{mo}. Substituting Eq. (22) into Eq. (12)-(13), using Eqs. (19)-(20) and keeping only the linear terms in a_1, φ_{m1} we obtain:

$$a_1' = \left[\frac{\mu}{2} - \frac{3\mu}{8}a_0^2 + \frac{f_2}{4\omega}\sin\varphi_{20}\right]a_1 + \left[\frac{f_1}{2\omega}\cos\varphi_{10} + \frac{f_2}{2\omega}a_0\cos\varphi_{20}\right]\varphi_{11} \quad (23)$$

$$\varphi_{11}' = \left[\frac{\sigma_1}{a_0} + \frac{\omega G}{2a_0} - \frac{9\lambda}{8\omega}a_0 - \frac{50\beta}{32\omega}a_0^3 + \frac{f_2}{4\omega a_0}\cos\varphi_{20}\right]a_1 - \left[\frac{f_1}{2\omega a_0}\sin\varphi_{10} + \frac{f_2}{2\omega}\sin\varphi_{20}\right]\varphi_{11} \quad (24)$$

The stability of a particular fixed point with respect to perturbations proportional to $\exp(\lambda t)$ depends on the real parts of the roots of the matrix. Thus, a fixed point given by equations (23)-(24) is asymptotically stable if and only if the real parts of all roots of the matrix are negative. Solid/dotted lines denote stable/unstable solution on the response curves, respectively.

NUMERICAL SIMULATIONS

Results are presented in graphical forms as steady state amplitudes against detuning parameters and as time history or the response of the system. A good criterion of both stability and dynamic chaos is the phase-plane trajectories, which are shown for some cases. In the following sections, the effects of the different parameters on response and stability will be investigated.

Time Histories

Fig. 1 shows the time histories of the system without controller at non-resonance case. The various parameters of the system in Fig. 1 are $\omega \cong 2.5, \Omega_1 = 2.2, \Omega_2 = 4.4, f_1 = 0.06, f_2 = 0.03, \mu = -0.01, \lambda = 0.04, \beta = 0.01$. It is clear that the system steady state amplitude is about 0.0429, and the phase plane shows a limit cycle, denoting that the system is free from chaos. Different initial conditions were tried and it was found that the system steady state amplitude is insensitive to the initial conditions.

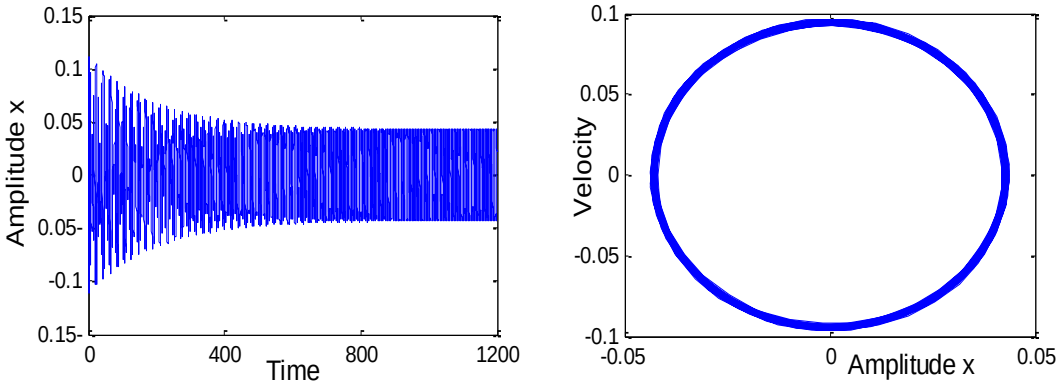

Figure 1. System behavior without controller at non resonance.

$$\omega \cong 2.5, \Omega_1 = 2.2, \Omega_2 = 4.4, f_1 = 0.06, f_2 = 0.03, \mu = -0.01, \lambda = 0.04, \beta = 0.01, G = 0.$$

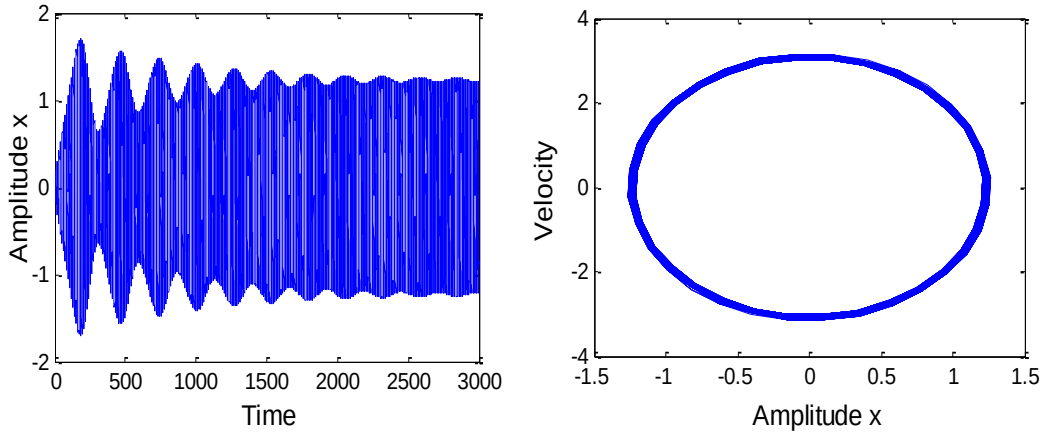

Figure 2. System behavior without controller at simultaneous primary and principal parametric resonance

$$\Omega_1 \cong \omega, \ \Omega_2 \cong 2\omega, G = 0.$$

$$\omega \cong 2.5, \Omega_1 = 2.5, \Omega_2 = 5, f_1 = 0.06, f_2 = 0.03, \mu = -0.01, \lambda = 0.04, \beta = 0.01.$$

Fig. 2 shows that the time response and phase plane of the simultaneous primary and principal parametric resonance case where $\Omega_1 \cong \omega, \ \Omega_2 \cong 2\omega$. It is observed that from this figure, we have that the system steady state amplitude is increased to about 1.27 and the oscillation becomes tuned. Figs. 3 and 4 illustrate the results when the controller is effective for different values of feedback gain *G*. It can be seen from Fig. 4 that the system steady state amplitude is reduced to about 0.008. This means that the effectiveness of the absorber Ea (Ea=steady state amplitude of the main system without controller/steady state amplitude of the main system with controller) is about 150.

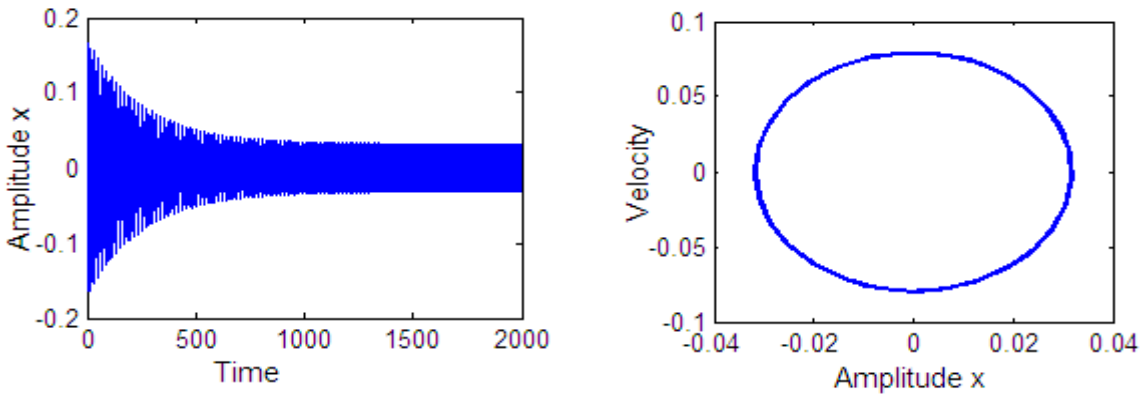

Figure 3. System behavior with controller at simultaneous primary and principal parametric resonance $\Omega_1 \cong \omega,\ \Omega_2 \cong 2\omega,$ $G = 0.3.$

$$\omega \cong 2.5, \Omega_1 = 2.5, \Omega_2 = 5, f_1 = 0.06, f_2 = 0.03, \mu = -0.01, \lambda = 0.04, \beta = 0.01.$$

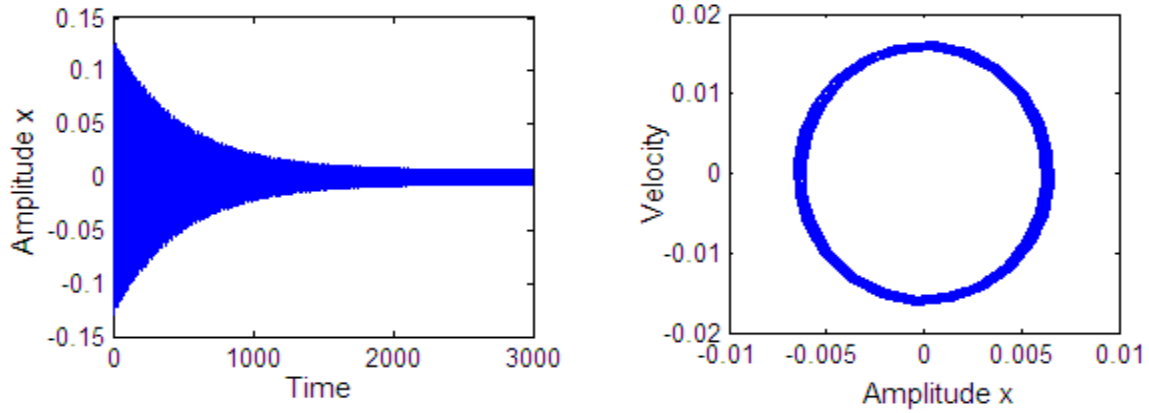

Figure 4. System behavior with controller at simultaneous primary and parametric resonance $\Omega_1 \cong \omega,\ \Omega_2 \cong 2\omega,\ G = 1.5$.

$$\omega \cong 2.5, \Omega_1 = 2.5, \Omega_2 = 5, f_1 = 0.06, f_2 = 0.03, \mu = -0.01, \lambda = 0.04, \beta = 0.01.$$

Effects of Different Parameters on System Behavior

In this section, the figures 5 to 10 are showing the effects of different parameters on the system response. The selected values for system parameters are the same values shown in Fig. 2. Figs. 5 to 8 show that the system steady state amplitude is a monotonic decreasing function to the feedback control gain *G*, natural frequency ω, non-linear parameters $\lambda, \beta,$ respectively. For greater values of $G, \omega, \lambda, \beta,$ leads to saturation phenomena as shown in Figs. 5 to 8. Figs. (9-10) shows that the steady state amplitude is a monotonic increasing function to the external and parametric excitation forces. For large values of excitation forces, the system exhibit unstable steady state motions.

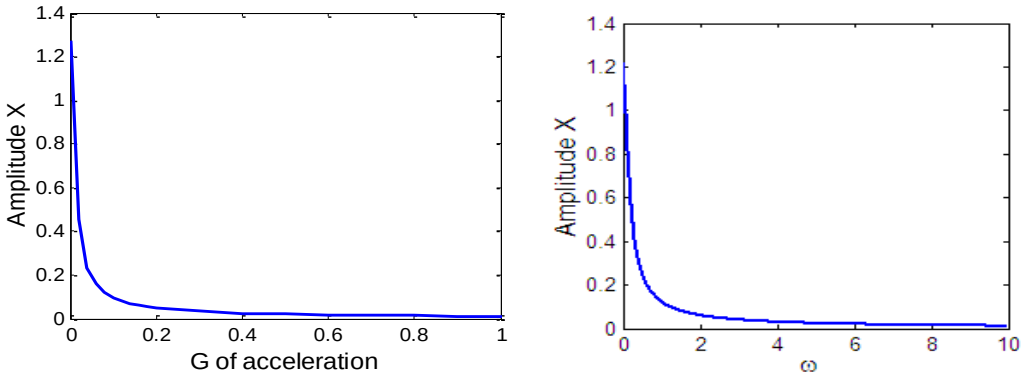

Figure 5. Effects of non-linear parameter α_2. Fig. 6. Effects of natural frequency ω.

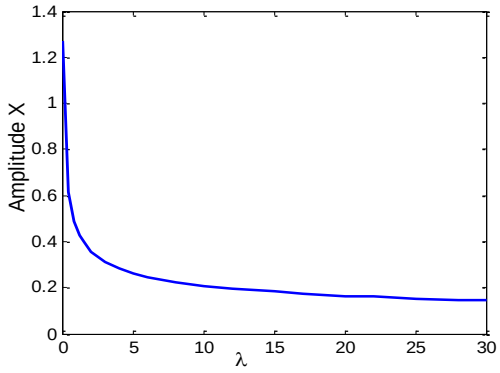

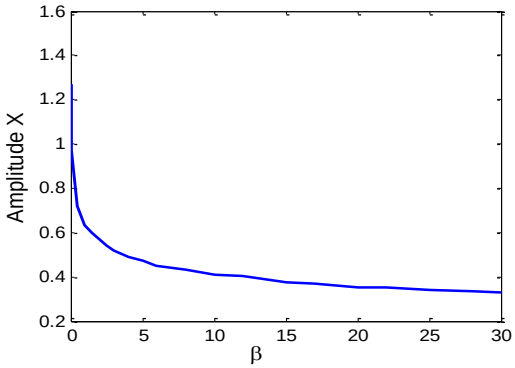

Figure 7. Effects of non-linear parameter λ. Fig. 8. Effects of non-linear parameter β.

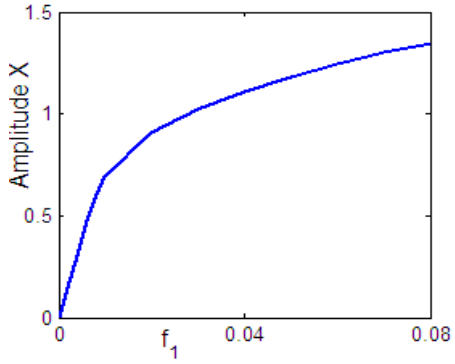

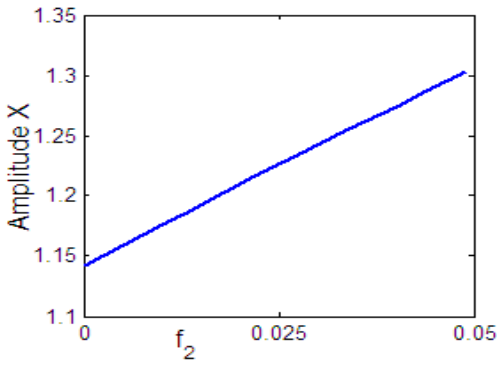

Figure 9. Effects of external excitation f_1. Fig. 10. Effects of parametric excitation f_2.

Frequency, Force Response Curves

In the following section, the steady state response of the system is investigated extensively for different parameters under simultaneous primary and principal parametric resonance. Results are presented in graphical forms as steady state amplitude against the detuning parameter σ and the excitation force f_1, by adopting the following values of the system parameters

$\omega \cong 2.5, \Omega_1 = 2.5, \Omega_2 = 5, f_1 = 0.06, f_2 = 0.03, \mu = -0.01,$

$\lambda = 0.04, \beta = 0.01,\ G = 0,$ which is the same values of the parameters shown in Fig. 2. Solid dark lines correspond to stable solutions, while dotted red ones correspond to unstable solutions. Fig. 11 shows the effects of the detuning parameter σ on the steady state amplitude of the system. In this figure, the response amplitude consists of a continuous curve which is bent to the right and has hardening phenomenon and there exist jump phenomenon. This continuous curve has stable and unstable solutions. At $\sigma = 0$ (simultaneous primary and principal parametric resonance $\Omega_1 \cong \omega, \Omega_2 \cong 2\omega$) the steady state amplitude is about 1.27 which is in good agreement with the Fig. 2.

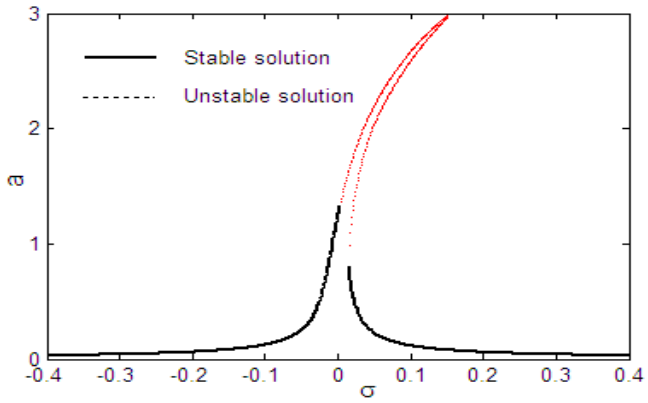

Figure 11. Effects of detuning parameter σ

$\omega \cong 2.5, \Omega_1 = 2.5, \Omega_2 = 5,\ f_1 = 0.06,\ f_2 = 0.03, \mu = -0.01, \lambda = 0.04, \beta = 0.01.$

The influence of the non-linear parameters β and λ on the frequency response curves of the system is presented in Fig. 12 and 13, respectively. Figs. 12 and 13 shows that positive and negative values of β and λ, produce either hard or soft spring respectively as the curve is either bent to the right or to the left, leading the appearance of the jump phenomenon. Also, it can be seen that from these figures that the steady state amplitude of the system is a monotonic decreasing function in

the non-linear parameters β and λ, this behavior is in agreement with the response curves in Figs. 4 and 5 respectively. Figs. 14 and 15 show the frequency response curves for various levels of the external and parametric excitation amplitude, f_1 and f_2, respectively. We notes that, when excitation amplitudes increased the frequency response curves bent away from the linear curves, producing multi-valued regions and jump phenomenon occurs. The steady state amplitude and the region of instability are increased for increasing f_1 and f_2, as shown in Figs. 14 and 15, this behavior is in agreement with the response curves in Figs. 6 and 7 respectively.

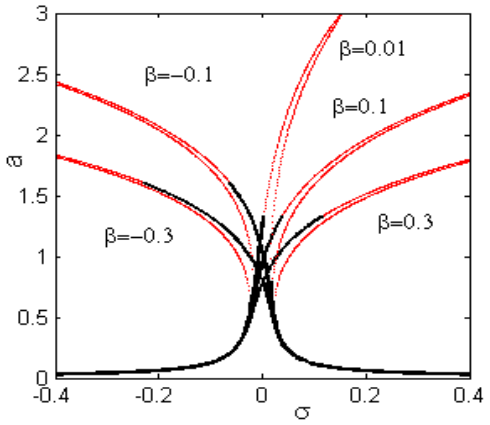

Figure 12. Effects of non-linear parameter β.

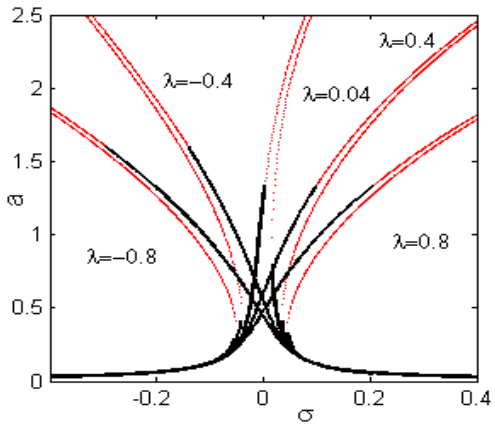

Figure 13. Effects of non-linear parameter λ.

For increasing value of the gain of the control G, the curve of the frequency response is shifted to the right as shown in Fig. 16. If the external and parametric forces excites the system at a frequency $\Omega_1 \cong \omega, \Omega_2 \cong 2\omega$, then this value as in the figure corresponds a maximum steady state amplitude on the curve (G=0) and less amplitude on the curve (G=0.07) and much less amplitude on the curve (G=0.14). An idea of tuning can be achieved by measuring the excitation frequencies, which gives us the value of detuning parameter σ from Eq. (10), then adding this value to the feedback gain G to be the new tuned one $G + \sigma$. Hence, we can warranty that the maximum steady state amplitude of controlled system will be shifted by the value of G to the left of any value of σ. This will make the controller adaptive with any change of excitation frequency and reduce the amplitude to a good minimum level. Fig. 17 shows that for decreasing value of natural frequency ω the curve is bent to the right, leading to multi-valued amplitude and to appearance of the jump phenomenon. It is clear that from Fig. 17 that the steady state amplitude is a monotonic decreasing function in ω, this behavior is in agreement with the response curves in Fig. 6.

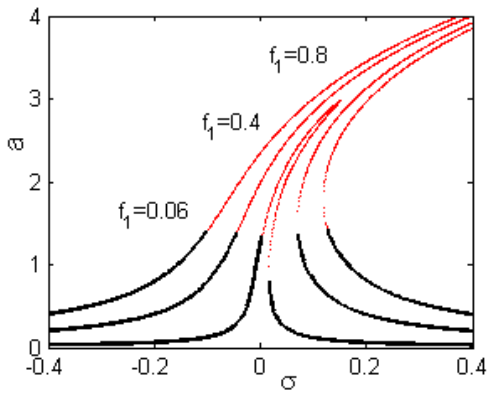

Figure 14. Effects of external excitation force f_1.

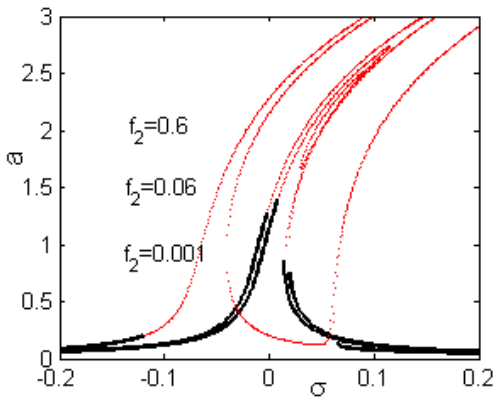

Figure 15. Effects of parametric excitation force f_2.

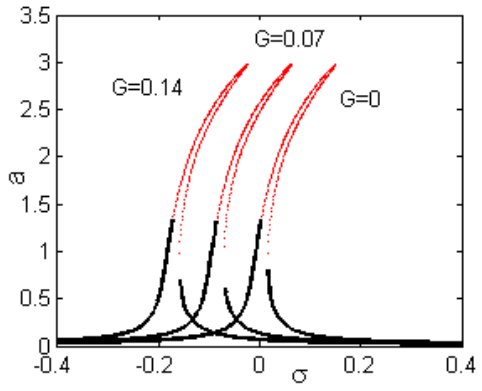

Figure 16. Effects of feedback gain G.

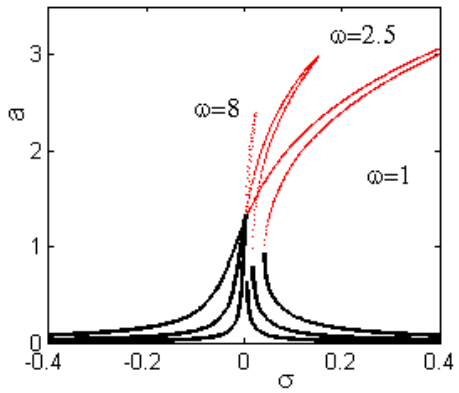

Figure 17. Effects of natural frequency ω.

Figs. 18 to 20 represent force–response curves for the non-linear solution of the case of simultaneous primary and principal parametric resonance case of the system. In these figures the amplitudes of the system are plotted as functions of the external excitation force f_1. Fig. 18 shows that the response amplitude of the system has a continuous curve and there exist zone of multi-valued solutions. There exists jump phenomenon and the curve has stable and unstable solutions for increasing positive detuning parameter σ. Increasing positive detuning parameter σ, means that decreasing natural frequency ω since $\Omega_1 = \omega + \varepsilon\sigma_1$, $\Omega_2 = 2\omega + \varepsilon\sigma_2$, $\sigma = \sigma_1 = \sigma_2/2$ then the jump phenomenon appears, this is agreement with Fig. 17. For large negative value of detuning parameter σ this means that increasing natural frequency ω then the jump phenomenon disappears and the curve has stable solution only. It is clear from Figs. 19 and 20 that for increasing non-linear parameters β, λ the steady state amplitude is decreasing with increasing regions of stability, this behavior is in agreement with the response curves in Figs.12 and 13, respectively.

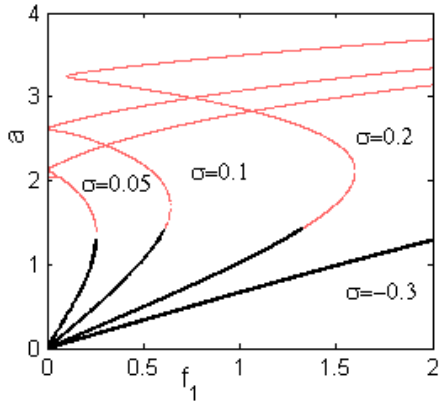

Figure 18. Force-response curves for varying detuning parameter σ.

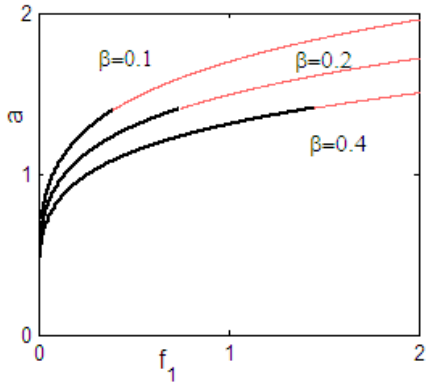

Figure. 19. Force-response curves for increasing on-linear parameter β.

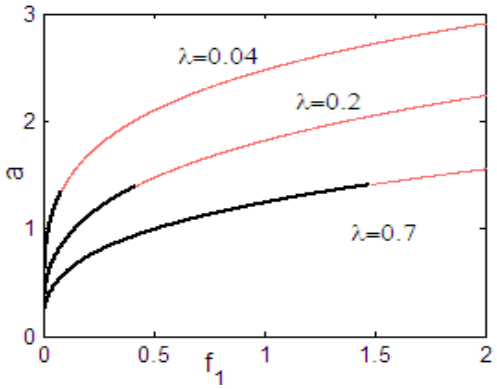

Figure 20. Force-response curves for increasing non-linear parameter λ.

Three cases of active control will be applied numerically to improve the behavior of the system at the simultaneous primary resonance case, via negative displacement feedback or negative velocity feedback or negative acceleration feedback. Fig. 21 shows a comparison between these three cases. It can be seen from the figure that all three cases leads to saturation phenomena for large values of *G*. Comparing the effectiveness of the three methods we can see that:

a) For negative displacement feedback, Ea =30

b) For negative velocity feedback, Ea =75

c) For negative acceleration feedback, Ea =150

It is clear that best of them for negative acceleration feedback.

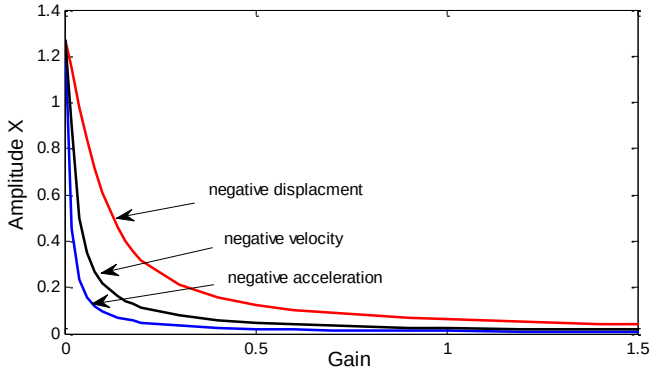

Figure 21. Effects of different feedback control.

Comparison between Analytical Solution Using Multiple Time Scale Method and Numerical Solution Using Runge Kutta Method

Figures 22 to 24 show a comparison between the time histories of the system approached by numerically integrating equation (1) and the approximate modulated amplitude of the system approached by numerically integrating equations (12)-(13). The dark dashed line represents the approximate modulated amplitude while the blue line represents the time history. The solutions presented in the graphs were obtained at the same values of the parameter system as shown in Fig. 2, except the external excitation force f_1 and the feedback gain G . Fig. 22, for $G = 0,$ and Fig. 23, for $G = 0.3,$ and Fig. 24, for $f_1 = 0.1$. The plotted approximate modulated amplitude describes closely the transient response of each time history.

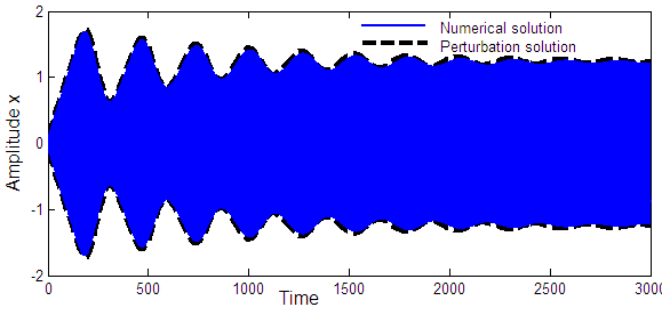

Figure 22. Comparisons between multiple time scale method and runge kutta method at simultaneous primary and principal parametric resonance $\Omega_1 \cong \omega,\ \Omega_2 \cong 2\omega, G = 0.$

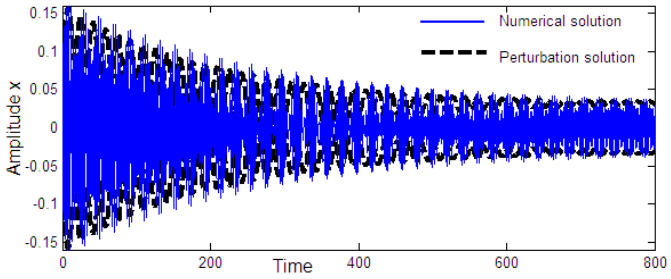

Figure 23. Comparisons between multiple time scale method and runge kutta method at simultaneous primary and principal parametric resonance $\Omega_1 \cong \omega,\ \Omega_2 \cong 2\omega, G = 0.3.$

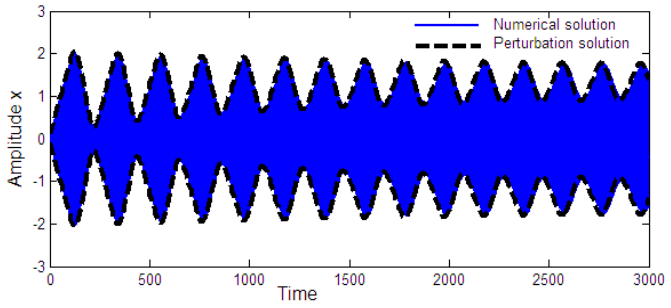

Figure 24. Comparisons between multiple time scale method and runge kutta method at simultaneous primary and principal parametric resonance $\Omega_1 \cong \omega,\ \Omega_2 \cong 2\omega, f_1 = 0.1$

Another comparison, to validate the results of multiple time scales perturbation analysis, the analytical results were verified by integration numerically of the original equation (1), and the numerical results for steady state solutions are marked as small circles on Fig. 25. Fig. 25 show a comparison between the frequency response curve for the system a , and the numerical simulation done to integrate Eq. (1) for the same parameters shown in Fig. 2. The dark solid lines correspond to stable solutions and dotted lines correspond to unstable solutions resulted from multiple time scale method, while the circles refer to the numerical integration. Figs. 26 to 29, shows a comparison between analytical solution using multiple time

scale and numerical solutions using integration of the system for f_1, G, β, λ, respectively.

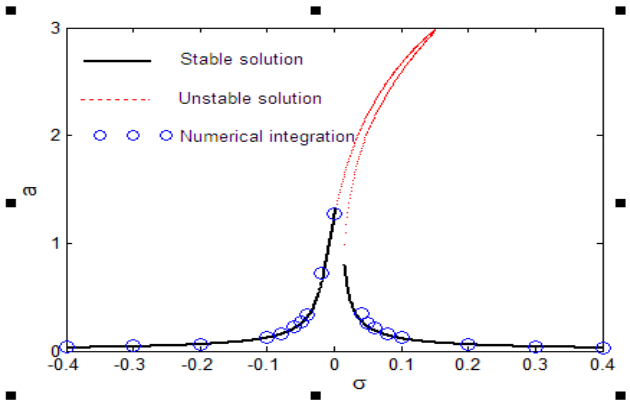

Figure 25. The frequency-response curves of the system at the same values of different parameters shown in Fig. 2. $\omega \cong 2.5, \Omega_1 = 2.5, \Omega_2 = 5,\ f_1 = 0.06,\ f_2 = 0.03, \mu = -0.01, \lambda = 0.04, \beta = 0.01.$

Figs. 25 to 29 showed that all predictions from analytical solutions are in very good agreement with the numerical simulation.

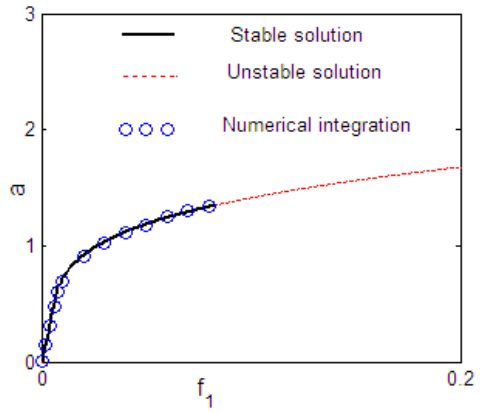

Figure 26. Effects of varying excitation force f_1 on the response.

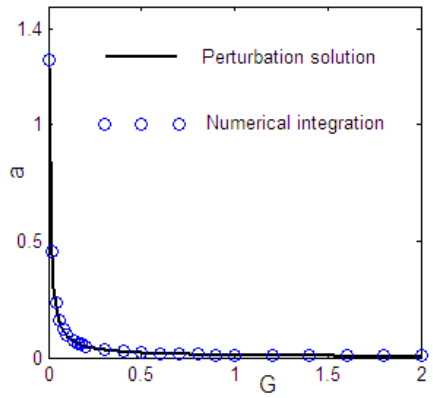

Figure 27. Effects of varying feedback control *G* on the response.

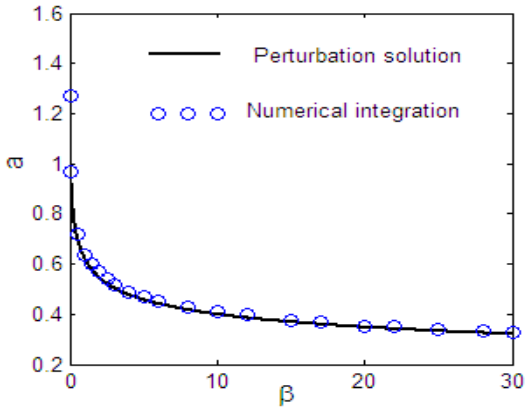

Figure 28. Effects of varying non-linear parameter β on the response.

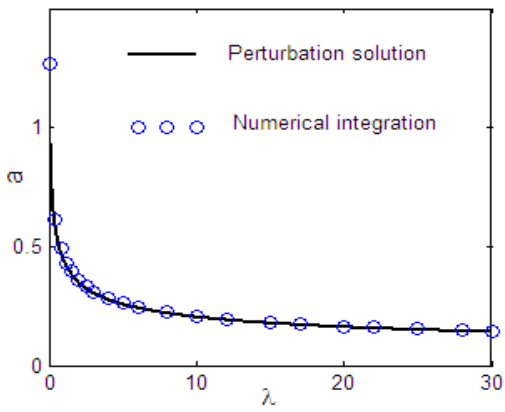

Figure 29. Effects of varying non-linear parameter λ on the response.

CONCLUSIONS

In this paper, the feedback controller was applied to eliminate the vibration of the Van der Pol equation subjected to external and parametric excitation forces at simultaneous primary and principal parametric resonance. Multiple time scale is applied to determine approximate solution for the system. The frequency, force response equations and the phase plane technique are applied to study the stability of the system. The bifurcation analysis was conducted to examine the stability of the system and to investigate the performance of the feedback control law. From the above study, the following may be concluded:

- The simultaneous resonance case $\Omega_1 \cong \omega, \Omega_2 \cong 2\omega$ is one of the worst resonance cases and it should be avoided in design.
- For large values of feedback gain, the controller is very suitable for vibration reduction.
- For positive and negative values of the nonlinear parameters $\beta, \lambda,$ the curves are bent to right or left leading to the occurrence of the jump phenomena and multi-valued amplitudes produce either hard or soft spring respectively.
- The steady state amplitude of the system is a monotonic increasing function in the excitation amplitudes f_1 and f_2.
- The region of stability increase, which is desirable, for increasing nonlinear parameters $\beta, \lambda,$ and for decreasing external and parametric excitation forces.
- The analytical solutions are in good agreement with the numerical integrations as in Figs. 22 to 28.
- Negative acceleration feedback active controller is the best one for the simultaneous resonance case $\Omega_1 \cong \omega, \Omega_2 \cong 2\omega$ as it reduces the vibration dramatically, as shown in Fig. 21.

REFERENCES

[1] J. A. González, L. E. Guerrero, A. Bellorín, Self-excited soliton motion, *Physical Review E*, **54** (1996), 1265–1273.

[2] V. I. Gulyayev, E. Y. Tolbatov, Forced and self-excited vibrations of pipes containing mobile boiling fluid clots, *Journal of Sound and Vibration*, **257** (2002), 425–437.

[3] X. J. Dai, J. P. Dong, Self-excited vibration of a rigid rotor rubbing with the motion-limiting stop, *International Journal of Mechanical Sciences*, **47** (2005), 1542–1560.

[4] Y. Ueda, N. Akamatsu, Chaotically transitional phenomena in the forced negative resistance oscillator, *IEEE Transactions, Circuits and Systems*, **28**, 3 (1981), 217–224.

[5] W. Szemplinska-Stupnicka, J. Rudowski, Neimark bifurcation almost-periodicity and chaos in the forced Van der Pol-duffing system in the neighbourhood of the principal resonance, *Physics Letters A*, **192**, (2–4) (1994), 201–206.

[6] A. Venkatesan, M. Lakshmanan, Bifurcation and chaos in the double-well Duffing–Van der Pol oscillator: numerical and analytical studies, *Physical Review E*, **56**, 6 (1997), 6321–6330.

[7] F. M. M. Kakmeni, S. Bowong, C. Tchawoua, E. Kaptouom, Strange attractors and chaos control in a Duffing–Van der Pol oscillator with two external periodic forces, *Journal of Sound and Vibration*, **277**, (4–5) (2004), 783–799.

[8] D. Liu, H. Yamaura, Chaos control of a ϕ^6 Van der Pol oscillator driven by external excitation, *Nonlinear Dynamics*, **68** (2012), 95–105.

[9] L. Ruihong, X. Wei, L. Shuang, Chaos control and synchronization of the ϕ^6 Van der Pol system driven by external and parametric excitations, *Nonlinear Dynamics*, **53** (2008), 261–271.

[10] J. Warminski, M. Bochenski, W. Jarzyna, P. Filipek, M. Augustyinak, Active suppression of nonlinear composite beam vibrations by selected control algorithms, *Communication in Nonlinear Science and Numerical Simulation*, **16** (2011), 2237–2248.

[11] K. Wang, S. Xiong, J. Zhang, Active vibration control of a flexible cantilever beam using piezoelectric actuators, *Energy Procedia*, **13** (2011), 4367–4374.

[12] J. Shan, H. Liu, D. Sun, Slewing and vibration control of a single-link flexible manipulator by positive position feedback (PPF), *Mechatronics*, **15**, 4 (2005), 487–503.

[13] WA. El-Ganaini, NA. Saeed, M. Eissa, Positive position feedback controller (PPF) for suppression of nonlinear system vibration, *Nonlinear Dynamics*, **72** (2013), 517–537.

[14] Y. A. Amer, H. S. Bauomy, M. Sayed, Vibration suppression in a twin-tail system to parametric and external excitations, *Computers and Mathematics with Applications*, **58** (2009), 1947–1964.

[15] M. Eissa, M. Sayed, A comparison between passive and active control of non-linear simple pendulum Part-I, *Mathematical and Computational Applications*, **11** (2006), 137–149.

[16] M. Eissa, M. Sayed, A comparison between passive and active control of non-linear simple pendulum Part-II, *Mathematical and Computational Applications*, **11** (2006), 151–162.

[17] M. Eissa, M. Sayed, Vibration reduction of a three DOF non-linear spring pendulum, *Communication in Nonlinear Science and Numerical Simulation*, **13** (2008), 465–488.

[18] M. Sayed, Improving the mathematical solutions of nonlinear differential equations using different control

methods, Ph. D. Thesis, Menofia University, Egypt, November (2006).

[19] M. Sayed, M. Kamel, Stability study and control of helicopter blade flapping vibrations, *Applied Mathematical Modelling*, **35** (2011), 2820–2837.

[20] M. Sayed, M. Kamel, 1:2 and 1:3 internal resonance active absorber for non-linear vibrating system, *Applied Mathematical Modelling*, **36** (2012), 310–332.

[21] M. Eissa, A. Kandil, M. Kamel, W. A. El-Ganaini, On controlling the response of primary and parametric resonances of a nonlinear magnetic levitation system, *Meccanica*, **50**, 1 (2015), 233–251.

[22] A. H. Nayfeh, *Introduction to Perturbation Techniques*, John Wiley & Sons, Inc., New York, 1993.

[23] A. H. Nayfeh, B. Balachandran, *Applied Nonlinear Dynamics*, John Wiley & Sons, Inc., New York, 1995.

A. H. Nayfeh, *Perturbation Methods*, John Wiley & Sons, Inc., 2000.